

See discussions, stats, and author profiles for this publication at: <https://www.researchgate.net/publication/6952966>

# Experimental and Theoretical Studies of the $C_2F_4 + O$ Reaction: Nonadiabatic Reaction Mechanism

ARTICLE in THE JOURNAL OF PHYSICAL CHEMISTRY A · NOVEMBER 2005

Impact Factor: 2.69 · DOI: 10.1021/jp053585y · Source: PubMed

CITATIONS

7

READS

19

5 AUTHORS, INCLUDING:



**Thanh Lam Nguyen**

University of Texas at Austin

72 PUBLICATIONS 1,382 CITATIONS

SEE PROFILE



**Bart Dils**

Belgian Institute for Space Aeronomy

44 PUBLICATIONS 293 CITATIONS

SEE PROFILE



**Jozef Peeters**

University of Leuven

205 PUBLICATIONS 4,455 CITATIONS

SEE PROFILE

## Experimental and Theoretical Studies of the $\text{C}_2\text{F}_4 + \text{O}$ Reaction: Nonadiabatic Reaction Mechanism

Thanh Lam Nguyen,<sup>†</sup> Bart Dils,<sup>‡</sup> Shaun Avondale Carl,<sup>†</sup> Luc Vereecken,<sup>†</sup> and Jozef Peeters<sup>\*,†</sup>

Department of Chemistry, University of Leuven, Celestijnenlaan 200F, B-3001 Leuven, Belgium, and Belgian Institute for Space Aeronomy, Avenue Circulaire 3, B-1180 Brussels, Belgium

Received: June 30, 2005

In this work, the  $\text{C}_2\text{F}_4(\text{X}^1\text{A}_g) + \text{O}(\text{P})$  reaction was investigated experimentally using molecular beam-threshold ionization mass spectrometry (MB-TIMS). The major primary products were observed to be  $\text{CF}_2\text{O}$  (+  $\text{CF}_2$ ) and  $\text{CF}_3$  (+  $\text{CFO}$ ), with measured approximate yields of  $84^{+7}_{-11}\%$  versus  $16^{+11}_{-7}\%$ , respectively, neglecting minor products. Furthermore, the lowest-lying triplet and singlet potential energy surfaces for this reaction were constructed theoretically using B3LYP, G2M(UCC, MP2), CBS-QB3, and G3 methods in combination with various basis sets such as 6-31G(d), 6-311+G(3df), and cc-pVDZ. The primary product distribution for the multiwell multichannel reaction was then determined by RRKM statistical rate theory and weak-collision master equation analysis. It was found that the observed production of  $\text{CF}_3$  (+  $\text{CFO}$ ) can only occur on the singlet surface, in parallel with formation of ca. 5 times more  $\text{CF}_2\text{O}(\text{X}) + \text{CF}_2(\text{X}^1\text{A}_1)$ . This requires fast intersystem crossing (ISC) from the triplet to the singlet surface at a rate of ca.  $4 \times 10^{12} \text{ s}^{-1}$ . The theoretical calculations combined with the experimental results thus indicate that the yield of triplet  $\text{CF}_2(\tilde{\text{a}}^3\text{B}_1) + \text{CF}_2\text{O}$  formed on the triplet surface prior to ISC is  $\leq 35\%$ , whereas singlet  $\text{CF}_2(\text{X}^1\text{A}_1) + \text{CF}_2\text{O}$  is produced with yield  $\geq 60\%$ , after ISC. In addition, the thermal rate coefficients  $k(\text{O} + \text{C}_2\text{F}_4)$  in the  $T = 150\text{--}1500 \text{ K}$  range were computed using multistate transition state theory and can be expressed as  $k(T) = 1.67 \times 10^{-16} \times T^{1.48} \text{ cm}^3 \text{ molecule}^{-1} \text{ s}^{-1}$ ; they are in agreement with the available experimental results in the  $T = 298\text{--}500 \text{ K}$  range.

### I. Introduction

In the series of  $\text{O} + \text{C}_2\text{H}_{4-x}\text{F}_x$  reactions, of importance in many combustion and plasma systems, the reaction between  $\text{O}(\text{P}) + \text{C}_2\text{F}_4(\text{X}^1\text{A}_g)$  is one of the extremes and shows interesting characteristics. Due to the weakening of the double bond (only  $70.4 \text{ kcal mol}^{-1}$ )<sup>1</sup> through F atom substitution, dissociation of the initial, triplet  $\text{C}_2\text{F}_4\text{O}$  adduct is believed to be very rapid, enabling the production of electronically excited  $\text{CF}_2(\tilde{\text{a}}^3\text{B}_1)$  together with  $\text{CF}_2\text{O}$  before intersystem crossing (ISC) can occur. The production of this electronically excited state has been confirmed by several groups, but further information on the primary product channels of the  $\text{O} + \text{C}_2\text{F}_4$  reaction is rather scarce. The reported values for the primary product yield ( $\eta$ ) of  $\text{CF}_2(\tilde{\text{a}}^3\text{B}_1)$  range between less than 1% and 85%. The reason for this large discrepancy is that these estimates are based on either the yield of products attributed to secondary  $\text{CF}_2(\tilde{\text{a}}^3\text{B}_1)$  reactions,<sup>2</sup> on  $\text{CF}_2(\tilde{\text{a}}^3\text{B}_1 \rightarrow \text{X}^1\text{A}_1)$  emission intensity vs time profiles,<sup>3</sup> or on  $\text{CF}_2(\tilde{\text{a}}^3\text{B}_1)/\text{CF}_2(\text{X}^1\text{A}_1)$  mass spectrometer signal ratios which had to be corrected for  $\text{CF}_2(\tilde{\text{a}}^3\text{B}_1)$  loss between formation and sampling.<sup>4</sup>

Direct accurate experimental product yield determinations are extremely difficult due to the nature of the products involved. Koda, however, succeeded in establishing upper and lower limits of the ratio of the radiative lifetime ( $\tau_{\text{rad}}$ ) over the yield ( $\eta$ ) of  $\text{CF}_2(\tilde{\text{a}}^3\text{B}_1)$ :  $0.19 \text{ s} < \tau_{\text{rad}}/\eta < 4 \text{ s}$ .<sup>5,6</sup> Other products channels have only been investigated by Dodonov et al.,<sup>4</sup> who reported a yield of  $17 \pm 8\%$  for  $\text{CF}_3(\text{X}^2\text{A}_1) + \text{CFO}(\text{X}^2\text{A}')$ .

Given this lack of data we set out to map all the primary product-formation pathways and to reduce the uncertainties on the yields of the various reaction products, in particular  $^3\text{CF}_2$ . For the  $\text{C}_2\text{H}_4 + \text{O}$  analogue, there is ample literature data<sup>7–21</sup> showing that this reaction proceeds partly on the initial triplet potential energy surface (PES) but partly also on a singlet PES after intersystem crossing (ISC); a 45:55 ratio of products formed from the triplet versus the singlet surface was found to describe the experimental data best.<sup>21</sup> Hence, it can be expected that the  $\text{C}_2\text{F}_4 + \text{O}$  reaction will also be affected by ISC; the heavier F atoms substituted for the H-atoms suggest that the ISC rate might even be significantly faster provided the  $\text{CF}_2$ - $\text{CF}_2\text{O}$  triplet and singlet electronic surfaces are as closely spaced as for the  $\text{CH}_2\text{CH}_2\text{O}$  system.<sup>21</sup> As far as we are aware, there are neither any quantum chemical calculations nor statistical kinetic analysis studies available in the literature on  $\text{C}_2\text{F}_4 + \text{O}$ .

In this work, we describe a theoretical study of the singlet and triplet PES for the  $\text{C}_2\text{F}_4 + \text{O}$  reaction at suitable levels of theory. These data were then used in a theoretical kinetic study of the product distribution of the  $\text{C}_2\text{F}_4 + \text{O}$  reaction using RRKM and weak-collision Master Equation theories, as detailed below. This theoretical work shows that formation of  $\text{CF}_3 + \text{CFO}$  products in the  $\text{C}_2\text{F}_4 + \text{O}$  reaction proceeds solely over the singlet surface, i.e., after an ISC event from the initial triplet surface. Hence, the yield of  $\text{CF}_3$  provides valuable information on the relative contributions of the triplet and singlet surfaces in the product formation in the reaction studied. We therefore performed an additional experimental mass-spectrometric study of the yield of  $\text{CF}_3 + \text{CFO}$  versus  $\text{CF}_2\text{O} + ^3\text{CF}_2/^1\text{CF}_2$  to verify the product distribution study by Dodonov et al.<sup>4</sup> These experimental product yields can then be combined with the

\* To whom correspondences should be addressed e-mail: Jozef.Peeters@chem.kuleuven.ac.be.

<sup>†</sup> University of Leuven.

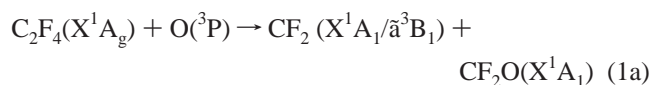
<sup>‡</sup> Belgian Institute for Space Aeronomy.

theoretical product distributions for the triplet and singlet surfaces to estimate the yield of triplet CF<sub>2</sub> in the title reaction.

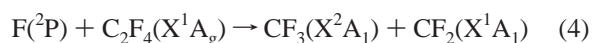
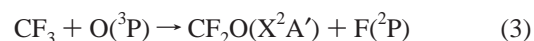
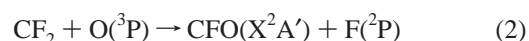
## II. Experimental Study

**II.1. Experimental Setup.** The discharge-flow/molecular beam sampling mass spectrometry apparatus (D-F/MBMS) applied in this work has been previously described in detail;<sup>22</sup> only a brief summary will be given here. The flow reactor consists of a cylindrical quartz tube ( $d = 1.65$  cm) equipped with a discharge sidearm, a concentric axially movable central injector tube, and an additional side inlet to admit carrier gas. Via these various inlets continuous flows of gases can be added to the flow reactor. Species concentrations in the reactor were determined from the fractional flows, the total pressure, and the temperature. A high-purity C<sub>2</sub>F<sub>4</sub> in He mixture is fed through the central movable injector tube and mixed with O atoms, which are generated far upstream by passing a flow of N<sub>2</sub>O diluted in He through a 50 W microwave discharge ( $\geq 98\%$  dissociation). All experiments were carried out at 295 K and at 3 Torr He. The 30 ms time lapse between O production and mixing with C<sub>2</sub>F<sub>4</sub> is largely sufficient to quench all O atoms to the <sup>3</sup>P ground state. Qualitative and quantitative analysis of the relevant species was carried out by molecular beam sampling and threshold-ionization mass spectrometry. At the reactor exit, the gas is sampled through a 0.3 mm pinhole in a quartz cone giving access to the first of two differentially pumped low-pressure chambers. The ensuing gas jet is mechanically modulated by a chopper in the first chamber to allow phase-sensitive detection. The resulting modulated molecular beam enters the second chamber, which houses a coaxial electron-impact ionizer and an extranuclear quadrupole mass spectrometer. For each single species of interest, the ionizing-electron energy  $E_{\text{el}}$  was adapted to avoid the unwanted contribution of possible fragment ions to the signal, i.e.,  $E_{\text{el}}$  was typically only a few eV above the ionization potential (IP) of the species being monitored. Thus, O was monitored at 15.0 eV electron energy, C<sub>2</sub>F<sub>4</sub> at 20 eV, N<sub>2</sub>O at 20 eV, CF<sub>3</sub> at 12.0 eV, and CF<sub>2</sub>O at 20 eV, unless specifically stated otherwise. A lock-in amplifier, tuned in phase with the beam modulation, allows distinction between the beam and background ions. Mass spectrometric sensitivities  $S(X)$  for stable molecules  $X$  in given experimental conditions of total gas pressure  $P$ , temperature  $T$ , etc., were determined separately by measuring MS signal intensities  $i(X)$  for known concentrations  $[X]$  established by feeding in known flows of  $X/\text{He}$  mixture and He carrier gas, at the given  $P$  and  $T$ .

**II.2. Experimental Methodology.** To determine whether CF<sub>3</sub> and CFO are formed as primary products, the possibility of formation through secondary reaction paths (see reactions 2 and 4 below) has to be eliminated. This requires low concentrations of O atoms and a high concentration of C<sub>2</sub>F<sub>4</sub>, that is, a very large ratio  $[\text{C}_2\text{F}_4]/[\text{O}]$ , such that all the O atoms react with C<sub>2</sub>F<sub>4</sub> and only a negligible fraction reacts with primary product radicals to form secondary CF<sub>3</sub> and CFO.



$$k_1 = (7.1 \pm 0.2) \times 10^{-13} \text{ cm}^3 \text{ molecule}^{-1} \text{ s}^{-1} \text{ (ref 6)}$$



$$k_4 = 4.8 \times 10^{-11} \text{ cm}^3 \text{ molecule}^{-1} \text{ s}^{-1} \text{ (ref 23)}$$

where CF<sub>2</sub> can either be in a singlet or triplet state. However, although the  $[\text{C}_2\text{F}_4]/[\text{O}]$  ratio was kept as high as possible ( $\sim 1000$ ), the possibility that the small observed CF<sub>3</sub> and CFO signals were (partly) secondary could not be excluded, since the rate constant of the secondary reaction of CF<sub>2</sub> with O ( $k_2 = 1.63 \times 10^{-11} \text{ cm}^3 \text{ molecule}^{-1} \text{ s}^{-1}$  for singlet CF<sub>2</sub><sup>24</sup> and  $k_{2*} = 3.4 \times 10^{-11} \text{ cm}^3 \text{ molecule}^{-1} \text{ s}^{-1}$  for triplet CF<sub>2</sub><sup>25</sup>) is almost 2 orders of magnitude higher than that of the primary reaction ( $k_1 = 7.1 \times 10^{-13} \text{ cm}^3 \text{ molecule}^{-1} \text{ s}^{-1}$ ).<sup>5,6</sup> To verify that CF<sub>3</sub> and CFO are indeed primary products, the evolution of the CF<sub>3</sub> concentration was monitored as a function of the added O atom concentration,  $[\text{O}]_0$ . At very low  $[\text{O}]_0$ , the dependence should be linear in case of primary CF<sub>3</sub> formation, while contributions via a secondary reaction path such as the sequence of reactions 2 and 4 should exhibit a quadratic  $[\text{CF}_3] \sim [\text{O}]_0^2$  dependence.

To maintain tight control over the O atom concentration and to avoid any potential interference from O<sub>2</sub>, the O atoms were created by dissociating N<sub>2</sub>O in the microwave discharge, since the  $\text{O}(\text{}^3\text{P}) + \text{N}_2$  yield of this process is almost unity ( $> 0.98$ ) as we established earlier.<sup>26</sup> To determine  $[\text{O}]_0$ , the MS signal intensity of N<sub>2</sub>O was measured, while the discharge was switched off (and therefore no dissociation into O-atoms occurs). Turning the discharge on dissociates all N<sub>2</sub>O into  $\text{O}(\text{}^3\text{P}) + \text{N}_2$ ; in the experimental conditions, no residual N<sub>2</sub>O signal was observed, nor was any NO detected, and therefore  $[\text{O}]_0$  is equal to the  $[\text{N}_2\text{O}]_i$  determined with the discharge off. As outlined above, the MS sensitivity to N<sub>2</sub>O was determined separately by feeding known flows of a N<sub>2</sub>O/He mixture and He carrier into the reactor and measuring the N<sub>2</sub>O signal intensities ( $m/e = 44$ ,  $E_{\text{el}} = 20$  eV).

Figure 1 (see also Table S6 in the Supporting Information (SI)) demonstrates that  $i(\text{CF}_3)$  exhibits a linear dependence toward initial  $[\text{O}]$  for small  $[\text{O}]_0$ . This proves conclusively that CF<sub>3</sub>, and therefore also CFO, are indeed primary products. The small abscissa-intercept, of  $\approx 7 \times 10^{11} \text{ molecule cm}^{-3}$ , could be attributed to a small background signal at  $m/e = 44$ , likely a trace of a few ppm CO<sub>2</sub> in the He carrier gas or the C<sub>2</sub>F<sub>4</sub>/He mixture.

Similar recordings were also made for CF<sub>2</sub>O, which is formed in the primary reaction 1a together with CF<sub>2</sub>. Again, the CF<sub>2</sub>O signals were measured for varying initial concentrations of O atoms at an identical high  $[\text{C}_2\text{F}_4]$  as above. Analyzing Figure 2 (and Table S7 in the Supporting Information), one can definitely conclude that CF<sub>2</sub>O and therefore CF<sub>2</sub> are produced in the primary C<sub>2</sub>F<sub>4</sub> + O reaction. The CF<sub>2</sub>O signal shows perfect linearity with respect to  $[\text{O}]_0$  over the experimental  $[\text{O}]_0$  concentration range. The small abscissa intercept, of  $7 \times 10^{11} \text{ molecule cm}^{-3}$ , is identical to that in the  $i(\text{CF}_3)$  versus  $[\text{O}]_0$  plots of Figures 1 and 2, showing that a small  $m/e = 44$  background signal is the common cause. The contribution of the secondary reaction 3 is therefore insignificant in the given  $[\text{O}]_0$  region. The wide  $[\text{O}]_0$  range over which  $i(\text{CF}_2\text{O})$  exhibits this linear behavior indicates that CF<sub>2</sub>O and hence also its coproduct CF<sub>2</sub> are the dominant primary products.

To evaluate the yields of the primary reaction channels 1a and 1b, we adopted equal mass spectrometric sensitivities ( $S_X$

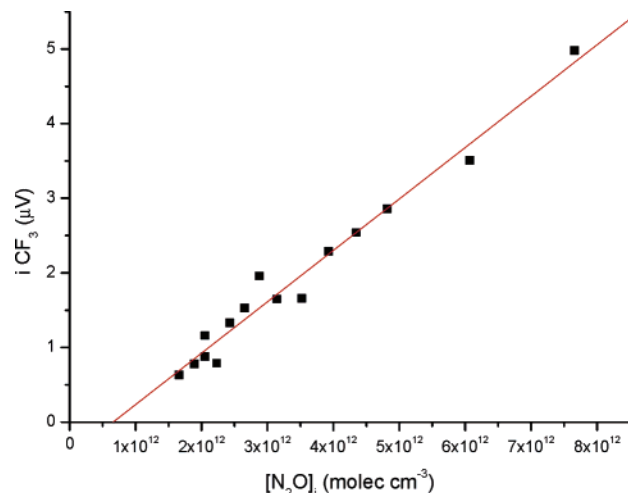


**Figure 1.** Mass spectrometric  $\text{CF}_3$  signal in function of O-atom concentration equal to initial  $[\text{N}_2\text{O}]_0$ ;  $[\text{C}_2\text{F}_4]_0 = 4.8 \times 10^{15} \text{ molecule cm}^{-3}$ ,  $t_r = 4 \text{ ms}$ ,  $p_{\text{tot}} = 3 \text{ Torr}$  (He carrier gas).

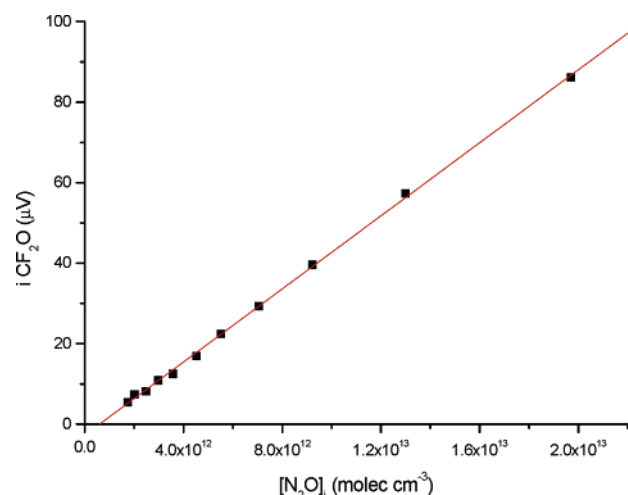


**Figure 2.** Mass spectrometric  $\text{CF}_2\text{O}$  signal in function of O-atom concentration = initial  $[\text{N}_2\text{O}]_0$ ;  $[\text{C}_2\text{F}_4]_0 = 4.8 \times 10^{15} \text{ molecule cm}^{-3}$ ,  $t_r = 4 \text{ ms}$ ,  $p_{\text{tot}} = 3 \text{ Torr}$  (He carrier).

$\equiv i(\text{X})/[\text{X}]$ ) for  $\text{CF}_2\text{O}$  and  $\text{CF}_3$  at equal excess electron energy ( $E_{\text{el}}$ ) above their respective ionization potentials (IP). This approximation stems from the widely applied quasi-additivity of atomic cross sections for electron impact ionization;<sup>27</sup> the error is expected to be small ( $\pm 30\%$ ) in this particular case, as  $\text{CF}_3$  and  $\text{CF}_2\text{O}$  are very similar in most respects. For the present yield ratio determination, the signals for  $\text{CF}_3$  and  $\text{CF}_2\text{O}$  were measured both at  $E_{\text{el}} 4.1 \text{ eV}$  in excess of their respective IP:<sup>28</sup>  $\text{IP}_{\text{CF}_3} = 8.9 \text{ eV}$ ,  $i(\text{CF}_3)$  measured at  $13 \text{ eV}$ ; and  $\text{IP}_{\text{CF}_2\text{O}} = 13.0 \text{ eV}$ ,  $i(\text{CF}_2\text{O})$  measured at  $17.1 \text{ eV}$ . The obtained signal intensities were as follows:  $i(\text{CF}_3) = 7.22 \mu\text{V} \pm 0.05 \mu\text{V}$  and  $i(\text{CF}_2\text{O}) = 38.1 \mu\text{V} \pm 1.5 \mu\text{V}$ , which leads to the following yields of primary  $\text{CF}_3$  and  $\text{CF}_2\text{O}$ :

$$\eta(\text{CF}_3 + \text{CFO}) = 16_{-7}^{+11}\%$$

$$\eta(\text{CF}_2\text{O} + \text{CF}_2) = 84_{-11}^{+7}\%$$

The errors allow for a conservative uncertainty estimate of a factor 2 on the relative sensitivities of the pertaining species.

This result is in excellent agreement with the  $k_{1b}/k_{1a}$  ratio of  $0.2 \pm 0.1$ , corresponding to  $\eta(\text{CF}_3 + \text{CFO}) = 17 \pm 8\%$  and  $\eta(\text{CF}_2\text{O} + \text{CF}_2) = 83 \pm 8\%$ , obtained by Dodonov et al.<sup>4,25</sup> based on their measurement of the initial linear portions of the

kinetic  $[\text{CF}_2]/[\text{C}_2\text{F}_4]$  and  $[\text{CF}_3]/[\text{C}_2\text{F}_4]$  curves in the  $\text{C}_2\text{F}_4 + \text{O}$  reaction, corrected for the contribution of secondary F-atom reactions whose concentration was monitored separately.

### III. Theoretical Methods

**III.1. Quantum Chemical Calculations.** Local minima and transition structures (TS) on the potential energy surfaces (PES) were initially optimized using density functional theory with the hybrid B3LYP functional<sup>29,30</sup> in conjunction with the 6-311+G(3df) basis set.<sup>31</sup> Analytical harmonic vibrational frequencies were then computed at this level in order to verify the character of the stationary points located (one imaginary frequency for a TS and all real frequencies for a minimum). Zero-point energies were used unscaled to correct the relative energies, and intrinsic reaction coordinate (IRC)<sup>32,33</sup> calculations at the lower B3LYP/6-31G(d) level (using the five “pure d” basis functions) establish the correct connections between the reaction intermediates; all IRC calculations are given in Figures S3–S12 in the Supporting Information. To obtain more accurate relative energies, the G2M(UCC,MP2) method<sup>34</sup> was used to compute single-point electronic energies based on the B3LYP/6-311+G(3df) optimized geometries. Additionally, the CBS-QB3<sup>35</sup> and G3<sup>36</sup> methods were also used. The values computed at the G2M(UCC,MP2), CBS-QB3, and G3 levels are in good agreement with each other, within  $1\text{--}2 \text{ kcal mol}^{-1}$ , and with experimental data where available (see Table 1). In this paper, we adopt the average of the values computed at these three levels of theory for the kinetic analysis. A possible error of  $\pm 2 \text{ kcal mol}^{-1}$  in relative energies was assumed to estimate the error in the computed product distributions.

Several stationary points have wave functions that are strongly perturbed by spin-contamination effects in the unrestricted formalism and/or have T1 diagnostic values much larger than 0.02 in the CCSD calculations, which is the recommended safe limit.<sup>37</sup> The wave functions of these structures are likely to possess a multireference character or near-degeneracy. In these cases the multireference CASSCF(8,8) method, in combination with the correlation consistent cc-pVDZ basis set,<sup>31</sup> was used to reoptimize geometries and to perform analytical Hessian calculations. Yet, the CASSCF calculations confirmed that for each of the species considered in this paper (see the Supporting Information) the HF-configuration is dominant (i.e. the CI-coefficient of the most important configuration is  $\geq 0.9$ ), indicating that a single-reference method should still give fair results. For a set of constrained optimizations with fixed CCO angles (see below), the CASSCF(8,8)/cc-pVDZ method was employed, and the energies were refined by including dynamic electronic correlations using the CASPT2(8,8)/cc-pVDZ method.

The B3LYP-DFT, G2M(UCC,MP2), CBS-QB3, and G3 calculations were performed using the Gaussian 03 package,<sup>38</sup> the CASSCF geometries and vibrational frequencies were computed using Dalton,<sup>39</sup> and the CASSCF constrained optimizations and CASPT2 energies were computed using Molpro 2002.<sup>40</sup>

**III.2. RRKM/Master Equation Calculations.** According to the statistical RRKM theory of unimolecular reaction rates,<sup>41–46</sup> the microcanonical rate constant  $k(E)$  for a reactant with internal energy  $E$  can be expressed as

$$k(E) = \frac{\alpha}{h} \times \frac{G^\ddagger(E - E^\ddagger)}{\rho(E)} \quad (5)$$

where  $\alpha$  is the reaction pathway degeneracy,  $h$  is Planck’s constant,  $E^\ddagger$  is the barrier height for the reaction,  $G^\ddagger(E - E^\ddagger)$  is



**TABLE 1: Computed Relative Energy (kcal mol<sup>-1</sup>) at 0 K for Various Species in the C<sub>2</sub>F<sub>4</sub>(D<sub>2h</sub>,X<sup>1</sup>A<sub>g</sub>) + O(<sup>3</sup>P) Reaction Using Different Levels of Theory**

species	B3LYP <sub>L</sub> <sup>a</sup>	G2M-b <sup>b</sup>	CBS-QB3	G3	average <sup>c</sup>	exp <sup>e</sup>
C <sub>2</sub> F <sub>4</sub> (D <sub>2h</sub> ,X <sup>1</sup> A <sub>g</sub> ) + O( <sup>3</sup> P)	0.0	0.0	0.0	0.0	0.0	0.0
CF <sub>2</sub> (C <sub>2v</sub> , <sup>3</sup> B <sub>1</sub> ) + F <sub>2</sub> CO(C <sub>2v</sub> ,X <sup>1</sup> A <sub>1</sub> )	-35.7	-32.4	-32.5	-33.1	-32.7	-32.7 ± 1
CF <sub>2</sub> (C <sub>2v</sub> ,X <sup>1</sup> A <sub>1</sub> ) + F <sub>2</sub> CO(C <sub>2v</sub> ,X <sup>1</sup> A <sub>1</sub> )	-88.2	-88.9	-89.3	-89.2	-89.2	-89.3 ± 1
CF <sub>3</sub> (C <sub>3v</sub> ,X <sup>2</sup> A <sub>1</sub> ) + CFO(C <sub>s</sub> ,X <sup>2</sup> A')	-56.1	-52.0	-51.9	-51.9	-51.9	-50.7 ± 3
F(X <sup>2</sup> P) + F <sub>2</sub> CCFO(C <sub>s</sub> ,X <sup>2</sup> A')	-29.2	-23.9	-25.8	-26.1	-25.3	
F(X <sup>2</sup> P) + CF <sub>3</sub> CO(C <sub>s</sub> ,X <sup>2</sup> A')	-22.9	-24.1	-23.3	-23.9	-23.8	
CO(C <sub>∞h</sub> ,X <sup>1</sup> Σ <sup>+</sup> ) + CF <sub>4</sub> (T <sub>d</sub> ,X <sup>1</sup> A <sub>1</sub> )	-140.5	-148.2	-147.9	-147.5	-147.9	-150 ± 4.8
C <sub>2</sub> F <sub>4</sub> O(C <sub>i</sub> , <sup>3</sup> A), Int1	-44.8	-43.1	-42.8	-43.1	-43.0	
F <sub>3</sub> CCFO(C <sub>i</sub> , <sup>3</sup> A), Int2	-47.2	-46.2	-45.6	-46.0	-45.9	
c-C <sub>2</sub> F <sub>4</sub> O(C <sub>2v</sub> ,X <sup>1</sup> A <sub>1</sub> ), Int3	-105.5	-110.3	-112.1	-111.0	-111.1	
F <sub>3</sub> CCFO(C <sub>s</sub> ,X <sup>1</sup> A'), Int4	-137.3	-141.5	-142.7	-142.4	-142.2	
TS1(C <sub>s</sub> , <sup>3</sup> A')	-6.4	1.1; 1.6 <sup>c</sup>	-0.3	0.5	0.4	
TS2(C <sub>s</sub> , <sup>3</sup> A')	-31.5	-27.1	-27.3	-28.3	-27.5	
TS3(C <sub>i</sub> , <sup>3</sup> A)	-30.8	-19.4	-22.5	-21.6	-21.2	
TS4(C <sub>i</sub> , <sup>3</sup> A)	-2.5	7.4	6.2	7.2	6.9	
TS5(C <sub>i</sub> , <sup>3</sup> A)	-39.7	-34.8	-35.5	-35.4	-35.2	
TS6(C <sub>i</sub> , <sup>3</sup> A)	-16.4	-2.9	-4.2		-3.6	
TS7(C <sub>s</sub> , <sup>1</sup> A')	-78.2	-78.3	-78.8	-78.8	-78.6	
TS8(C <sub>i</sub> , <sup>1</sup> A)	-72.4	-71.0	-71.7	-72.0	-71.6	
TS9(C <sub>i</sub> , <sup>1</sup> A)	-51.4	-51.6	-51.7	-52.9	-52.1	
TS10(C <sub>i</sub> , <sup>1</sup> A) <sup>d</sup>	-67.7	-61.6	-64.1	-61.9	-62.5	

<sup>a</sup> B3LYP<sub>L</sub> stands for B3LYP/6-311+G(3df). <sup>b</sup> G2M-b = CCSD(T)/6-311+G(d)//B3LYP<sub>L</sub> + [MP2/6-311+G(3df)//B3LYP<sub>L</sub> - MP2/6-311+G(d)//B3LYP<sub>L</sub>] + ZPE[B3LYP<sub>L</sub>], where B3LYP<sub>L</sub> stands for B3LYP/6-311+G(3df) optimized geometry. G2M-a = CCSD(T)/6-311G(d)//B3LYP<sub>L</sub> + [MP2/6-311+G(3df)//B3LYP<sub>L</sub> - MP2/6-311G(d)//B3LYP<sub>L</sub>] + ZPE[B3LYP<sub>L</sub>]. <sup>c</sup> Average = (G2M + CBS-QB3 + G3)/3. <sup>d</sup> Variational transition state located at the C–C distance in CF<sub>3</sub>CFO(C<sub>s</sub>,X<sup>1</sup>A') of 2.7 Å for the CF<sub>3</sub>CFO(C<sub>s</sub>,X<sup>1</sup>A') → CF<sub>3</sub>(C<sub>3v</sub>,X<sup>2</sup>A<sub>1</sub>) + CFO(C<sub>s</sub>,X<sup>2</sup>A') channel. <sup>e</sup> <http://srdata.nist.gov/cccbdb/>, all values derived at 0 K from those at 298 K: ΔH<sub>f</sub><sup>0</sup>(<sup>3</sup>O) = 58.98 kcal mol<sup>-1</sup>; ΔH<sub>f</sub><sup>0</sup>(C<sub>2</sub>F<sub>4</sub>) = -156.81 kcal mol<sup>-1</sup>; ΔH<sub>f</sub><sup>0</sup>(CF<sub>2</sub>) = -44.12 kcal mol<sup>-1</sup>; ΔH<sub>f</sub><sup>0</sup>(CF<sub>2</sub>) = -12.48 kcal mol<sup>-1</sup>; ΔH<sub>f</sub><sup>0</sup>(CF<sub>2</sub>O) = -143 kcal mol<sup>-1</sup>; ΔH<sub>f</sub><sup>0</sup>(CF<sub>3</sub>) = -112.14 kcal mol<sup>-1</sup>; ΔH<sub>f</sub><sup>0</sup>(CFO) = -36.4 ± 3 kcal mol<sup>-1</sup>; ΔH<sub>f</sub><sup>0</sup>(CO) = -27.2 kcal mol<sup>-1</sup>; ΔH<sub>f</sub><sup>0</sup>(CF<sub>4</sub>) = -221.6 ± 4.8 kcal mol<sup>-1</sup>.

the sum of vibration states of the transition structure for energies from 0 up to  $E - E^\ddagger$ , and  $\rho(E)$  is the density of vibration states for a reactant molecule with internal energy  $E$ .

Some of the vibrational modes calculated for the stationary points correspond to internal rotations around the C–C axis in the molecule; their harmonic vibrational frequency is typically much smaller than 100 cm<sup>-1</sup>. These modes were treated as free internal rotors, a fair approximation for the chemically activated OC<sub>2</sub>F<sub>4</sub> adducts of interest here, as the barriers for internal rotation are only about 1.5–2.0 kcal mol<sup>-1</sup> for all cases (calculated at B3LYP/6-311+G(3df) level of theory), while the average energy content per internal degree of freedom is 3 kcal mol<sup>-1</sup> (triplet OC<sub>2</sub>F<sub>4</sub>) to 7–8 kcal mol<sup>-1</sup> (singlet OC<sub>2</sub>F<sub>4</sub>). The sum and density of states in eq 5 are now taken as the convolution of the density of a classical one-dimensional free rotor with the sum and density of states of the vibration modes<sup>43,46</sup>

$$k(E) = \frac{\alpha \int_0^{E-E^\ddagger} G_v^\ddagger(E-E^\ddagger-x) \rho_r^\ddagger(x) dx}{h \int_0^E \rho_v(E-y) \rho_r(y) dy} \quad (6)$$

where  $\rho_r$  is the density of states of the classical one-dimensional free rotor which can be computed<sup>46</sup> as  $\rho_r(E) = (B \times E)^{-1/2}$ , where  $B$  is the internal rotational constant. The Beyer–Swinehart algorithm<sup>47,48</sup> was used to compute the sum and density of states in eq 6 employing a grain size of 1 cm<sup>-1</sup>.

For the barrierless CF<sub>3</sub>CFO(X<sup>1</sup>A') → CF<sub>3</sub>(X<sup>2</sup>A<sub>1</sub>) + CFO(X<sup>2</sup>A') exit channel, variational transition state theory<sup>43–46</sup> was used to locate the kinetic bottleneck. The UB3LYP/6-311+G-(3df) level of theory was employed to optimize geometries and calculate vibrational frequencies along the reaction coordinate (RC) using constrained optimizations with fixed C–C bond lengths in CF<sub>3</sub>–CFO(X<sup>1</sup>A'); energies along the RC were refined at the G2M level of theory. Using this PES,  $k(E)$  rate coefficients at every position along the RC were computed for internal

energies  $E$  of 137.3 or 141.5 kcal mol<sup>-1</sup> corresponding to the decrease in potential energy of CF<sub>3</sub>–CFO relative to the reactants at the UB3LYP-DFT or G2M levels of theory, respectively (see Figure S12a,b in the Supporting Information). The minimal  $k(E)$  was found for a C–C bond distance of 2.7 Å, and the characteristics at this point along the RC were used in the subsequent kinetic calculations.

The product distribution for the O(<sup>3</sup>P) + C<sub>2</sub>F<sub>4</sub> reaction occurring on the separate adiabatic triplet or singlet surfaces was obtained by solution of the weak-collision master equation under various conditions ( $P = 10^{-3} - 1$  atm,  $T = 298 - 700$  K). The Lennard-Jones collision parameters for the bath gas He are  $\sigma = 2.55$  Å and  $\epsilon/k_B = 10$  K.<sup>49</sup> Since no collision parameters for [C<sub>2</sub>F<sub>4</sub>O] are available in the literature, the values  $\sigma = 4.08$  Å and  $\epsilon/k_B = 421$  K are estimated based on those of ethylene oxide C<sub>2</sub>H<sub>4</sub>O.<sup>49</sup> Thus, the collision frequency  $Z_{LJ}$  [ $M$ ] was estimated at  $\approx 1.1 \times 10^{10}$  s<sup>-1</sup> at 1 atm and room temperature. The probability density function for collision energy transfer was computed using the biexponential model of Troe.<sup>50</sup> An average energy transferred per collision  $\langle \Delta E \rangle_{\text{all}}$  of -130 cm<sup>-1</sup> was adopted.<sup>49</sup>

In the energy-grained master equation, the maximum energy considered was 200 kcal mol<sup>-1</sup> above the lowest conformer (e.g. CF<sub>3</sub>CFO(X<sup>1</sup>A')), and a small energy band size of 0.03 kcal mol<sup>-1</sup> was chosen to ensure that the density of states does not change significantly within the band. A stochastic simulation is used to solve the master equation following Gillespie's exact stochastic method (ESM).<sup>51–53</sup> To obtain product distributions with high precision, a large number of stochastic trials was chosen, usually 10<sup>7</sup>. The choice of a good random number generator is also very important in the stochastic simulation. In this application, RANLUX<sup>54,55</sup> having a very long period of 10<sup>165</sup> with a luxury level of 4 was chosen. A detailed explanation on the stochastic solution of the master equation was given in our earlier paper.<sup>56</sup>

**III.3. Theoretical Results and Discussions. III.3.1. Potential Energy Surface. The Triplet Electronic State.** According to the spin-conservation rule, the electrophilic addition reaction of triplet  $O(^3P)$  to singlet  $C_2F_4$  takes place on the triplet surface. Unless mentioned otherwise, the relative energies given below were obtained at the G2M, CBS-QB3, and G3 levels of theory, and the averages of these values were used for the kinetic computations. The  $O + C_2F_4$  reaction is initiated by a chain-addition on the  $C=C$  double bond in  $C_2F_4$  to form a vibrationally excited triplet  $OCF_2CF_2$  intermediate (denoted hereafter as **Int1**). An addition transition state does not exist at the B3LYP/6-311+G(3df) level of theory. However, previous experimental studies<sup>57–59</sup> indicate that the overall rate constant of the  $O(^3P) + C_2F_4$  reaction depends positively on temperature with an Arrhenius activation energy of  $0.6 \pm 0.2$  kcal mol<sup>-1</sup>.<sup>59</sup> IRCMax-(G2M(UCC,MP2):B3LYP/6-311+G(3df)),<sup>60</sup> IRCMax(CBS-QB3),<sup>60</sup> and IRCMax(G3) calculations were then carried out along the reaction coordinate within a  $C_s$  symmetry and a  $^3A''$  electronic state. An addition TS (denoted hereafter as **TS1**) was located at an O–C bond distance of 2.1 Å (see Figure S1 in the Supporting Information). **TS1** lies 1.1 and 0.5 kcal mol<sup>-1</sup> in energy above the initial reactants at the G2M and G3 levels, respectively, while at the CBS-QB3 level it lies 0.3 kcal mol<sup>-1</sup> below the reactants, always after ZPE-correction. These results indicate that this addition step has a very small or even nonexistent barrier. The average of these three values, 0.4 kcal mol<sup>-1</sup>, will be adopted for computing the overall rate coefficient  $k(T)$  (see below).

Triplet  $OCF_2CF_2$  **Int1** formed via the addition reaction mechanism above has no symmetry and lies 43.0 kcal mol<sup>-1</sup> lower than the reactants. Starting at **Int1**, there are three possible channels: (1) elongation of the C–C bond in **Int1** leading to products  $CF_2(^3B_1) + F_2CO$  via **TS2** of  $C_s$  symmetry and  $^3A''$  electronic state, presenting a barrier of 15.5 kcal mol<sup>-1</sup> (see Figure 3); (2) loss of an F atom from the  $CF_2$  moiety in **Int1** to form products  $F + F_2CCFO$  via **TS3** with a barrier height of 21.8 kcal mol<sup>-1</sup>; and (3) a simultaneous 1,2 F-shift and C–C bond breakage in **Int1** via **TS4** to form  $CF_3 + CFO$ , the most exothermic products on the triplet surface. **TS4** is a very tight transition structure and presents a huge barrier of 49.9 kcal mol<sup>-1</sup>, so this channel cannot compete with the former two. We were not successful in locating a TS directly connecting **Int1** to triplet  $CF_3CFO$  as all attempts always converged to either **TS3** or **TS4**. O’Gara and Dailey<sup>61</sup> calculated a barrier for 1,2-F migration in triplet 2,2,2-trifluoroethylidene of 50.8 kcal mol<sup>-1</sup> at the QCISD(T)/6-311G(2d,2p)//MP2/6-31G(d,p) level. If a direct TS for the **Int1**  $\rightarrow$   $^3CF_3CFO$  channel exists, this channel is expected to show a similarly high barrier and should therefore be negligible.

Thus, it is immediately apparent from Figure 3 that two channels should kinetically control the product formation on the triplet PES:  $O + C_2F_4 \rightarrow OCF_2CF_2 \rightarrow$  **TS2**  $\rightarrow CF_2(^3B_1) + F_2CO$  and  $O + C_2F_4 \rightarrow OCF_2CF_2 \rightarrow$  **TS3**  $\rightarrow F + F_2CCFO$ , with the former clearly expected to dominate. Primary production of  $CF_2(^3B_1)$  (+  $F_2CO$ ) was indeed observed in several experimental studies,<sup>2,4–6,25,62,63</sup> whereas  $F_2CCFO$  (+F) formation has not yet been reported.

It is of key importance to note here that  $CF_3 + CFO$  cannot be formed in any significant amounts from the triplet PES, presented in Figure 3. However, these products were reported to be formed in considerable yields by Dodonov et al.<sup>25</sup> and unambiguously confirmed as primary products with substantial yields in our experimental investigation (see above). The above

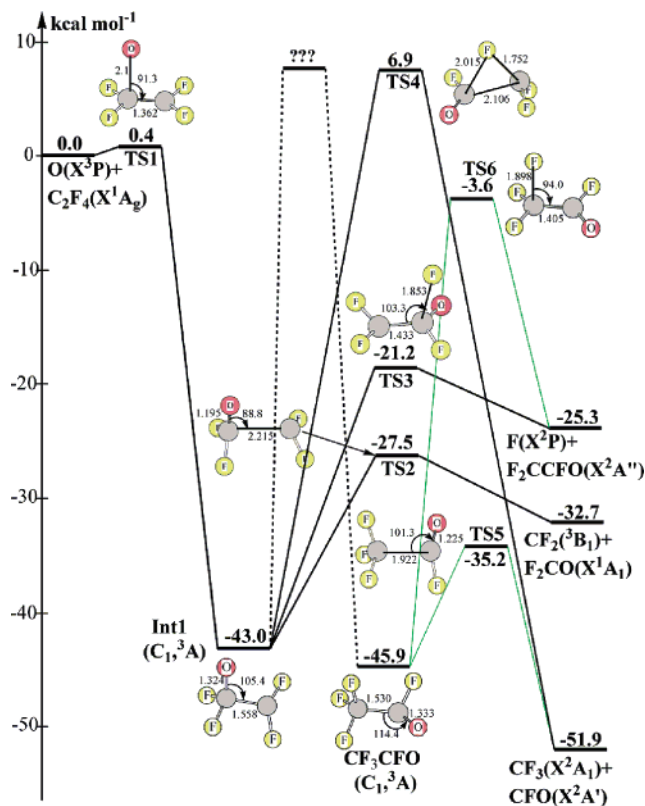


**Figure 3.** Potential energy surface for the  $O(^3P) + C_2F_4(X^1A_g)$  reaction on the triplet surface constructed using average relative energies computed at the G2M, CBS-QB3, and G3 levels of theory.

strongly indicates the need for a fast ISC event from the triplet to the singlet PES to describe the experimental product yields completely.

It is therefore of primordial interest to investigate the triplet-to-singlet crossing seam in the  $O(^3P) + C_2F_4$  reaction and to compare it with the ISC crossing in the  $O(^3P) + C_2H_4$  reaction, described earlier.<sup>21</sup> In both cases, the triplet  $\rightarrow$  singlet crossing occurs for the initial-adduct  $OCX_2-CX_2$  structures and is followed by a fast quasi-barrierless subsequent ring closure on the singlet surface characterized mainly by a decrease in the OCC angle. As shown for the  $C_2H_4O$  system,<sup>21</sup> normal stretching vibrations tend to have a similar parabolic energy profile without overly affecting the triplet-singlet PES energy gap, while the OCC bending coordinate will alter the geometries more and hence be the foremost coordinate affecting the energetic differences between triplet and singlet surfaces. Constrained optimizations for several fixed OCC angle were carried out at the CASSCF(8,8)/CASPT2(8,8)/cc-pVDZ level<sup>23</sup> for both the singlet and triplet surfaces (see Figure 4a for  $C_2H_4$  and Figure 4b for  $C_2F_4$ ). As can be seen in these figures, the  $C_2F_4O$  singlet/triplet surfaces overlap over a much wider range of OCC angles compared to the  $C_2H_4O$  system, such that the crossing space region in the title reaction is much wider, increasing the likelihood of crossing significantly. In addition, the fluorine atoms in  $C_2F_4$  are much heavier than the hydrogen atoms in  $C_2H_4$ , additionally enhancing surface crossing. Hence, we expect that the ISC process in the  $O(^3P) + C_2F_4$  reaction occurs much faster than for  $O(^3P) + C_2H_4$ , such that the ratio of triplet/singlet yields for the  $O(^3P) + C_2F_4$  reaction should be smaller than the value of 45/55 for the  $O(^3P) + C_2H_4$  reaction,<sup>21</sup> even when allowing for the shorter unimolecular-reaction lifetime of the hot triplet  $CF_2CF_2O$  adduct ( $\sim 1$  ps; ESM analysis of this work) as compared to that of  $CH_2CH_2O$  ( $\sim 8$  ps<sup>21</sup>).

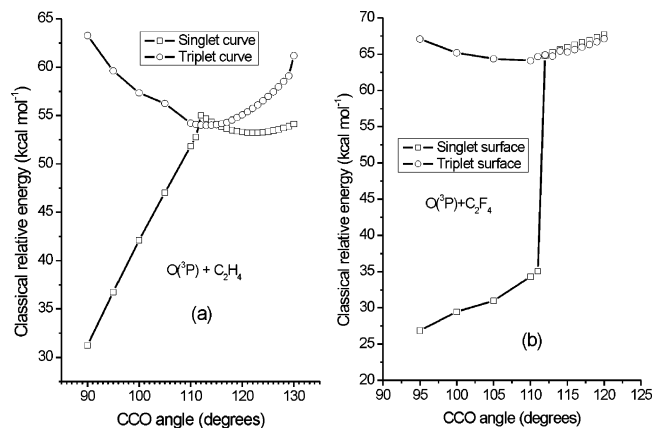


**Figure 4.** Constrained optimizations for several fixed OCC angles at the CASSCF(8,8)/CASPT2(8,8)/cc-pVDZ level of theory on the singlet and triplet surfaces for (a) the  $O(^3P) + C_2H_4$  reaction and (b) the  $O(^3P) + C_2F_4$  reaction.

**The Singlet Electronic State.** Intersystem crossing of the initial triplet  $\bullet O-CF_2-\bullet CF_2$  biradical **Int1** yields the singlet biradical  $\bullet O-CF_2-\bullet CF_2$  (denoted hereafter as **Int1s**). At the low UHF/6-31G(d) level of theory, we located the **Int1s** as a stationary point on the singlet surface, with relative energy 1.1 kcal mol<sup>-1</sup> above the triplet biradical **Int1**. However, **Int1s** does not appear as a local minimum at the more rigorous CASSCF(8,8)/cc-pVDZ level of theory; optimizations at this level always converge to the cyclic conformer singlet tetrafluorine ethylene oxide, **Int3** (see Figure 5). Additionally, constrained optimizations for several fixed CCO angles in **Int1s** (see Figure 13S in the Supporting Information) at the CASPT2//CASSCF level showed that there is indeed no barrier to cyclization, indicating that other processes (e.g. a 1,2 F-shift in **Int1s**) can certainly not compete with this ring-closure. Therefore, after ISC, the resulting **Int1s** will promptly relax to singlet tetrafluorine ethylene oxide (**Int3**). **Int3**,  $C_{2v}$  point group and a  $^1A_1$  electronic state, has an internal energy of 111.1 kcal mol<sup>-1</sup> relative to the initial reactants. Note that the fast relaxation to **Int3** moves intermediates away from the triplet  $\leftrightarrow$  singlet crossing seam, virtually eliminating the possibility of reverse ISC back to the triplet surface.

Starting at **Int3**, there are two accessible reaction channels: (1) decomposition to products  $CF_2(X^1A_1) + F_2CO$  via **TS7**, which has  $C_s$  symmetry and a  $^1A'$  electronic state and lies 32.5 kcal mol<sup>-1</sup> above **Int3** and (2) a concerted 1,2-F shift in combination with C–O bond breaking to form singlet tetrafluorine acetaldehyde  $CF_3CFO$  **Int4** via **TS8** with a barrier height of 39.5 kcal mol<sup>-1</sup>. The former pathway is slightly more favorable in energy. **Int4**, with a relative energy of 142.2 kcal mol<sup>-1</sup> below the initial reactants, of  $C_s$  point group and  $^1A'$  electronic state, can react in three possible ways, shown in Figure 5: (1) isomerization back to **Int3** via **TS8** with a barrier height of 70.6 kcal mol<sup>-1</sup>; (2) concerted 1,2-F migration combined with C–C bond scission leading to  $CF_4 + CO$  via **TS9**, which lies 90.1 kcal mol<sup>-1</sup> above **Int4**; and (3) fragmentation to products  $CF_3 + CFO$  via a (near-)barrierless transition state **TS10** (not shown in Figure 5), which is located 79.7 kcal mol<sup>-1</sup> above **Int4**. As the transition states for decomposition of **Int4** into reaction products lie much higher than that for the **Int3**  $\leftrightarrow$  **Int4** (re-)isomerization (see Figure 5), the efficiency of the second channel of **Int3**, above, will be further reduced. As a consequence,  $CF_2(X^1A_1) + F_2CO$  are expected to be the dominant products on the singlet surface.

**III.3.2. Product Distribution.** The partial product distributions from the triplet  $\bullet CF_2CF_2O\bullet$  and singlet oxirane adducts

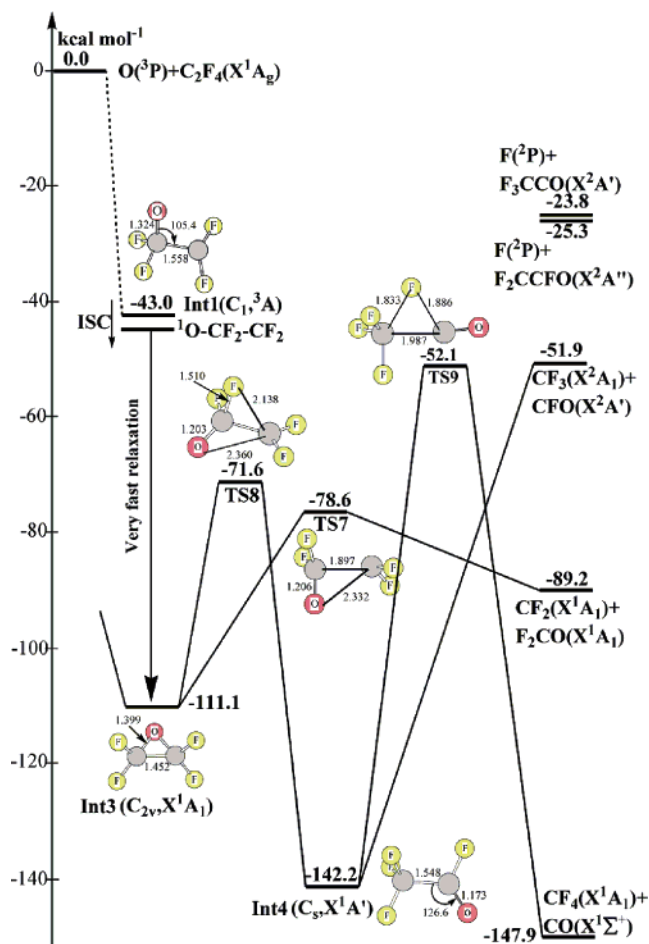


**Figure 5.** Potential energy surface for the  $O(^3P) + C_2F_4(X^1A_2)$  reaction occurring on the singlet surface constructed using average relative energies computed at the G2M, CBS-QB3, and G3 levels of theory. The triplet entrance part is shown by dashed lines.

were derived separately by solving the appropriate master equations independently. The initial energy distribution of formation of the triplet  $\bullet CF_2CF_2O\bullet$  adduct from  $O(^3P) + C_2F_4$  via **TS1** was derived from detailed balance considerations.<sup>42</sup> The results obtained under various reaction conditions ( $T = 298-700$  K and  $P = 10^{-3}-1$  atm) are presented in Tables 4S and 5S (see the Supporting Information).

**The Triplet Surface.** Computation of the product yields by ESM solution of the master equation for the selected reaction conditions  $P = 10$  Torr and  $T = 298$  K gives  $89.5^{+5.5}_{-9.5}\%$   $CF_2(^3B_1) + F_2CO$ , and  $10.5^{+9.5}_{-5.5}\%$   $F_2CCFO + F$ , whereas yields of all other products are negligible ( $<1\%$ ). The errors on the yields were evaluated by varying the **TS3** energy by 2 kcal mol<sup>-1</sup>. In fact, the yields are found to be invariant over the pressure range of  $<10^{-3}-1$  atm but to slightly change as a function of temperatures (see Table S4 in the Supporting Information). The yield of  $F_2CCFO + F$  increases from 10.5% at 298 K to 14.5% at 700 K at the expense of the  $CF_2(^3B_1) + F_2CO$  yield. The pressure-independence reflects the short unimolecular lifetime of the “hot” triplet adduct  $OCF_2CF_2$ , computed to be  $\approx 1$  ps, such that at pressures below 1 atm it suffers no collision energy losses.

**The Singlet Surface.** The product yields were computed by solving the ME, using the average relative energies from our G2M, CBS-QB3, and G3 calculations. The lifetime of the initial “hot” oxirane is estimated to be  $\approx 1.5$  ps, while it requires dozens of collisions to stabilize this adduct. As a result, the product distribution was likewise found to be independent of



**TABLE 2:** Calculated Overall Product Distribution (%) as a Function of the CF<sub>3</sub> Yield Observed in the Experiment at the Reaction Conditions of  $T = 298$  K and  $P = 10$  Torr

singlet products			triplet products	
CF <sub>3</sub> + CFO	CF <sub>2</sub> (X <sup>1</sup> A <sub>1</sub> ) + F <sub>2</sub> CO	CF <sub>4</sub> + CO	CF <sub>2</sub> (a <sup>3</sup> B <sub>1</sub> ) + F <sub>2</sub> CO	F( <sup>2</sup> P) + F <sub>2</sub> CCFO
8.0	53.2	0.3	34.5	4.0
9.0	59.9	0.4	27.5	3.2
10.0	66.5	0.4	20.7	2.4
11.0	73.2	0.4	13.8	1.6
12.0	79.8	0.5	6.9	0.8
13.0	86.5	0.5	0.0	0.0

pressure below 1 atm but to change slightly as a function of temperature. The computed yield of CF<sub>3</sub> + CFO increases from 12.9% at 298 K to 14.4% at 700 K, whereas the yield of CF<sub>2</sub>(X<sup>1</sup>A<sub>1</sub>) + F<sub>2</sub>CO decreases by about 1.8% (see Table S5 in the Supporting Information). For the reaction conditions of  $T = 298$  K and  $P = 10$  Torr, products yields were computed to be 86.5% CF<sub>2</sub>(X<sup>1</sup>A<sub>1</sub>) + F<sub>2</sub>CO, 12.9% CF<sub>3</sub> + CFO, and 0.6% CF<sub>4</sub> + CO, with an estimated error of  $\pm 5\%$ .

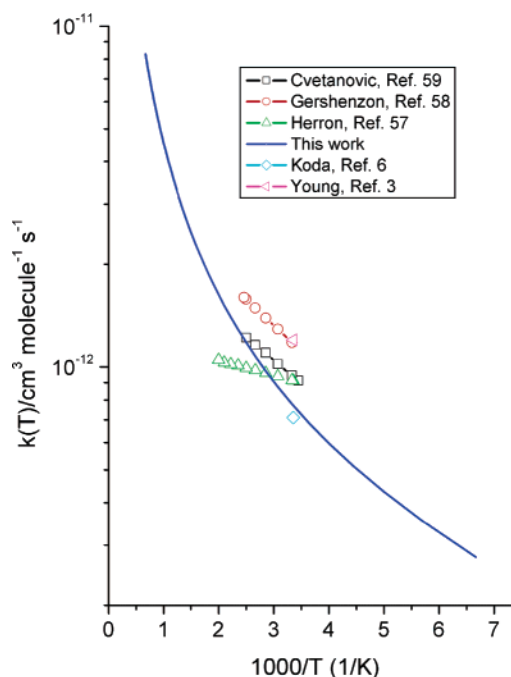
**Overall Primary Product Distribution.** To compute the overall product distribution, accounting for the rate of intersystem crossing between the triplet and singlet surfaces, one must know the ISC rate at the minimum in the seam of crossing (MSX)<sup>64</sup> between the triplet and singlet surfaces. To compute this rate, trajectory dynamic calculations, e.g. “on the fly” nonadiabatic dynamics,<sup>65</sup> are required. However, such calculations are far beyond the scope of this paper. Lacking accurate dynamic calculations, in this work we estimate the overall product distribution by matching the yield of CF<sub>3</sub> =  $16 \pm 8\%$  observed experimentally earlier by Donodov<sup>4</sup> and by us in this paper (see above). Overall product distribution was computed as a function of the CF<sub>3</sub> yield, varying from the experimental lower limit of 8% up to 13%; this latter upper limit requires 100% intersystem crossing according to our RRKM-ME results. The calculated results presented in Table 2 show that the CF<sub>2</sub>(X<sup>1</sup>A<sub>1</sub>) + F<sub>2</sub>CO and CF<sub>2</sub>(a<sup>3</sup>B<sub>1</sub>) + F<sub>2</sub>CO yields so found are highly sensitive to the adopted CF<sub>3</sub> yield. Increasing the CF<sub>3</sub> yield by 5%, from 8% to 13%, increases the yield of CF<sub>2</sub>(X<sup>1</sup>A<sub>1</sub>) by 33%, from 53% to 86%, whereas the CF<sub>2</sub>(a<sup>3</sup>B<sub>1</sub>) yield significantly reduces from  $\sim 34$  to 0%. It should be indicated that for the considered range of 8–13% CF<sub>3</sub>, the CF<sub>2</sub>(a<sup>3</sup>B<sub>1</sub>) yield cannot exceed 35%. Table 2 also shows that F<sub>2</sub>CCFO + F ( $< 4\%$ ) and CF<sub>4</sub> + CO ( $\approx 0.5\%$ ) are predicted to be minor products, insensitive to the adopted yield of CF<sub>3</sub>; neither of these two product channels has been observed experimentally. Our predicted total F<sub>2</sub>CO product yield of 87–88% is in excellent agreement with the experimental values of  $84^{+7}_{-11}\%$  observed by us and  $83\% \pm 8\%$  by Dodonov et al.<sup>4,25</sup>

Assuming a yield of 10% for CF<sub>3</sub>, product formation contributions from the triplet and singlet surfaces are predicted to be 20% and 80%, respectively. Using these contributions, we derive an ISC crossing rate of  $\approx 4 \times 10^{12} \text{ s}^{-1}$  from the triplet to the singlet surface using the RRKM-ESM lifetime of 1 ps found here for the triplet adduct  $\bullet\text{CF}_2\text{CF}_2\text{O}^\bullet$ .

**III.3.3. Overall Rate Coefficient.** The overall temperature-dependent rate coefficient  $k(T)_{\text{overall}}$  for the O(<sup>3</sup>P) + C<sub>2</sub>F<sub>4</sub> reaction can be computed as follows

$$k(T)_{\text{overall}} = (1 - \gamma_{\text{re}}) \times k_{\text{TST}}(T) \quad (7)$$

where  $k_{\text{TST}}(T)$  is the rate coefficient derived from transition state theory and  $\gamma_{\text{re}}$  is the yield of OCF<sub>2</sub>CF<sub>2</sub> redissociation back to the initial reactants, O(<sup>3</sup>P) + C<sub>2</sub>F<sub>4</sub>. The value of  $\gamma_{\text{re}}$  is a function

**Figure 6.** Overall thermal rate coefficients computed (TST) at temperatures in the range of 150–1500 K. Experimental data are given for the purpose of comparison.

of pressure and temperature; at the conditions considered ( $T = 298$ – $700$  K and  $P \leq 1$  atm) it is negligibly small (see Tables S4 and S5 in the Supporting Information) such that  $k(T)$  can be computed directly from the transition state theory expression

$$k(T)_{\text{overall}} = k(T)_{\text{TST}} = \alpha \times \frac{k_{\text{b}} T}{h} \times \frac{Q_{\text{TS}^\ddagger}(T)}{Q_{\text{O}}(T)Q_{\text{C}_2\text{F}_4}(T)} \exp(-E^\ddagger/RT) \quad (8)$$

where  $Q(T)$  is a complete partition function,  $k_{\text{b}}$  is Boltzmann’s constant,  $h$  is Planck’s constant,  $R$  is the universal gas constant,  $E^\ddagger$  is the barrier height of  $0.4 \text{ kcal mol}^{-1}$  (see higher) for the initial addition channel, and  $\alpha$  is the reaction path degeneracy obtained from the symmetry number ratio  $\sigma_{\text{C}_2\text{F}_4}/\sigma_{\text{TS}^\ddagger} = 4$ . The electronic partition function of the O atom explicitly includes the three lowest-lying electronic states (<sup>3</sup>P<sub>2</sub> (electronic degeneracy  $g = 5$ ), <sup>3</sup>P<sub>1</sub> ( $g = 3$ ), and <sup>3</sup>P<sub>0</sub> ( $g = 1$ )), with relative energies of 0.000, 0.453, and  $0.649 \text{ kcal mol}^{-1}$ , respectively.<sup>66</sup> The electronic degeneracy of 3 for **TS1**, which has a triplet electronic state, was duly taken into account.

Overall thermal rate coefficients in the wide range of temperatures 150–1500 K were computed and plotted in Figure 6, together with some of the available experimental data for comparison, showing a favorable comparison between our computed  $k(T)$  and the available experimental data<sup>57–59</sup> covering the range 298–500 K. Our computed rate constant of  $7.7 \times 10^{-13} \text{ cm}^3 \text{ molecule}^{-1} \text{ s}^{-1}$  at room temperature is in good agreement with the available experimental values of  $(7\text{--}13) \times 10^{-13} \text{ cm}^3 \text{ molecule}^{-1} \text{ s}^{-1}$ .<sup>3,6,57–59</sup> Our  $k(T)_{\text{overall}}$  is well-reproduced by the expression:  $k(T) = 1.64 \times 10^{-16} \times T^{1.48}$ .

It should be mentioned that for the reaction of O(<sup>3</sup>P) with halogenated ethylene systems (F<sub>2</sub>C=CXY, where X and Y = H, F, Cl, Br), a linear correlation between rate coefficients and ionization potentials (IP) has been reported, i.e., the larger IP the faster reaction rate.<sup>67–68</sup> F<sub>2</sub>C=CF<sub>2</sub> has the largest IP<sup>67</sup> and accordingly also the highest rate coefficient for the reaction with



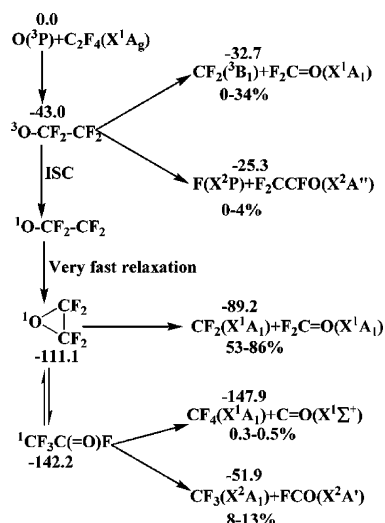


**Figure 7.** Recommended reaction mechanism for the  $O(^3P) + C_2F_4(X^1A_g)$  reaction. Reaction energies and overall product distribution are also given.

$O(^3P)$ . This trend is opposite with that in the reactions of  $O(^3P)$  with alkyl-substituted ethylenes.<sup>59</sup>

#### IV. Conclusions

The  $O(^3P) + C_2F_4(X^1A_g)$  reaction was investigated experimentally using discharge-flow techniques and molecular-beam-sampling threshold-ionization mass spectrometry as well as theoretically using various high levels of quantum theory followed by statistical rate RRKM – Master Equation analyses.

In the experimental study, we observed the major primary reaction products to be  $F_2CO$  (with coproduct  $CF_2$ , either triplet or singlet) and  $CF_3$  (with  $FCO$  or  $CO + F$  coproducts), in a ratio of ca. 0.84:0.16 with error margins  $\approx \pm 0.08$ , thus confirming the results of Dodonov et al.<sup>4</sup>

The computational results show that the observed product distribution necessitates a nonadiabatic reaction mechanism involving fast triplet  $\rightarrow$  singlet intersystem crossing of the initial  $F_2C-CF_2O$  adduct at a rate of ca.  $4 \times 10^{12} s^{-1}$ , with the majority of the products resulting from subsequent reactions on the singlet surface, to give an overall product distribution presented in Figure 7. This nonadiabatic reaction mechanism is similar to that of the  $O(^3P) + C_2H_4(X^1A_g)$  reaction.<sup>21</sup>

Our combined experimental and theoretical results show that both singlet and triplet  $CF_2$  can be produced in the  $O(^3P) + C_2F_4$  reaction, but with a preponderance of the singlet ground state, the yield of triplet  $CF_2$  being predicted to be at most 35% and possibly only a few percent.

Finally, overall thermal TST rate coefficients were computed for temperatures in the range of 150–1500 K; they can be expressed as  $k(T) = 1.64 \times 10^{-16} \times T^{1.48}$ . The  $k(T)$  results, derived entirely from first principles, are in agreement with the available experimental data.

**Acknowledgment.** The authors thank the FWO-Vlaanderen and the KULeuven-Research Council (BOF fund) for continuing financial support. L.V. and S.C. are postdoctoral fellows of the FWO-Vlaanderen, while T.L.N. holds a doctoral grant from the KULeuven Research Council.

**Supporting Information Available:** Optimized geometries, zero-point energies, total energies, relative energies, rotational constants, harmonic vibrational frequencies, the most important configuration coefficients in a wave function, and IRC calculations

computed at different levels of theory. This material is available free of charge via the Internet at <http://pubs.acs.org>.

#### References and Notes

- (1) Chase, M. W., Jr. *NIST-JANAF Thermochemical Tables, Fourth Edition*, J. Phys. Chem. Ref. Data, Monograph **1998**, 9, 1–1951.
- (2) Heicklen, J. *Adv. Photochem.* **1969**, 7, 57 and references therein.
- (3) Young, R. A.; Blauer, J.; Bower, R.; Lin, C. L. *J. Chem. Phys.* **1988**, 88, 4834.
- (4) Dodonov, A. F.; Zelenov, V. V.; Kukui, A. S. *Sov. J. Chem. Phys.* **1990**, 6, 3368.
- (5) Koda, S. *Chem. Phys. Lett.* **1978**, 55, 353.
- (6) Koda, S. *J. Phys. Chem.* **1979**, 83, 2065.
- (7) Yamaguchi, K.; Yabushita, S.; Fueno, T.; Kato, S.; Morokuma, K. *Chem. Phys. Lett.* **1980**, 70, 27.
- (8) Dupuis, M.; Wendoloski, J. J.; Takada, T.; Lester, W. A., Jr. *J. Chem. Phys.* **1982**, 76, 481.
- (9) Melius, C. F. *BAC-MP4 method* (see ref 14).
- (10) Fueno, T.; Takahara, Y.; Yamaguchi, K. *Chem. Phys. Lett.* **1990**, 167, 291.
- (11) Jursic, B. S. *Theochem* **1999**, 492, 85.
- (12) Endo, Y.; Tsuchiya, S.; Yamada, C.; Hirota, E.; Koda, S. *J. Chem. Phys.* **1986**, 85, 4446 and see references therein.
- (13) Bley, U.; Dransfeld, P.; Himme, B.; Koch, M.; Temps, F.; Wagner, H. G. *22th Symp. (Int.) Comb.* **1988**, 997.
- (14) Schmoltner, A. M.; Chu, P. M.; Brudzynski, R. J.; Lee, Y. T. *J. Chem. Phys.* **1989**, 91, 6926 and see references therein.
- (15) Koda, S.; Endo, Y.; Tsuchiya, S.; Hirota, E. *J. Phys. Chem.* **1991**, 95, 1241.
- (16) Knyazev, V. D.; Arutyunov, V. S.; Vedenev, V. I. *Int. J. Chem. Kine.* **1992**, 24, 545.
- (17) Abou-Zeid, O. K.; McDonald, J. D. *J. Chem. Phys.* **1998**, 109, 1293.
- (18) Quandt, R.; Min, Z.; Wang, X.; Bersohn, R. *J. Phys. Chem. A* **1998**, 102, 60.
- (19) Min, Z.; Wong, T. H.; Quandt, R.; Bersohn, R. *J. Phys. Chem. A* **1999**, 103, 10451.
- (20) Oguchi, T.; Ishizaki, A.; Kakuta, Y.; Matsui, H.; Miyoshi, A. *J. Phys. Chem. A* **2004**, 108, 1409 and see ref 14 therein.
- (21) Nguyen, T. L.; Vereecken, L.; Hou, X. J.; Nguyen, M. T.; Peeters, J. *J. Phys. Chem. A* **2005**, 109, 7489.
- (22) Boullart, W.; Devriendt, K.; Borms, R.; Peeters, J. *J. Phys. Chem.* **1996**, 100, 998.
- (23) Butkovskaya, N. L.; Larichev, M. N.; Leipunskii, I. O.; Morozov, I. I.; Talroze, V. L. *Kinet. Catal.* **1980**, 21, 263.
- (24) Yamasaki, K.; Tanaka, A.; Watanabe, A.; Yokoyama, K.; Tokue, I. *J. Phys. Chem.* **1995**, 99, 15086.
- (25) Dodonov, A. F.; Zelenov, V. V.; Kukui, A. S. *Sov. J. Chem. Phys.* **1991**, 7, 1089.
- (26) Peeters, J.; Langhans, I.; Boullart, W.; Nguyen, M. T.; Devriendt, K. *J. Phys. Chem.* **1994**, 98, 11988.
- (27) Ötvös, J. W.; Stevenson, D. P. *J. Am. Chem. Soc.* **1956**, 78, 546.
- (28) Rosenstock, H. M.; Draxl, K.; Steiner, B. W.; Herron, J. T. *J. Phys. Chem. Ref. Data* **1977**, 6, supplement no. 1.
- (29) Becke, A. D. *J. Chem. Phys.* **1993**, 98, 5648.
- (30) Stevens, P. J.; Devlin, F. J.; Chabowski, C. F.; Frisch, M. J. *J. Phys. Chem.* **1994**, 98, 11623.
- (31) EMSL Basis Set Library, <http://www.emsl.pnl.gov/forms/basis-form.html>
- (32) Gonzalez, C.; Schlegel, H. B. *J. Chem. Phys.* **1989**, 90, 2154.
- (33) Gonzalez, C.; Schlegel, H. B. *J. Phys. Chem.* **1990**, 94, 5523.
- (34) Mebel, A. M.; Morokuma, K.; Lin, M. C. *J. Chem. Phys.* **1995**, 103, 7414. The total energy of a molecular system is computed as follows:  $E[G2M(UCC, MP2)-a] = E[CCSD(T)/6-311G(d)/B3LYP_L] + \{E[MP2/6-311+G(3df)/B3LYP_L] - E[MP2/6-311G(d)/B3LYP_L]\} + ZPE[B3LYP_L]$ , where B3LYP\_L stands here for the geometries optimized at the B3LYP/6-311+G(3df) level of theory.  $E[G2M(UCC, MP2)-b] = E[CCSD(T)/6-311+G(d)/B3LYP_L] + \{E[MP2/6-311+G(3df)/B3LYP_L] - E[MP2/6-311+G(d)/B3LYP_L]\} + ZPE[B3LYP_L]$ .
- (35) Montgomery, J. A., Jr.; Frisch, M. J.; Ochterski, J. W.; Petersson, G. A. *J. Chem. Phys.* **1999**, 110, 2822.
- (36) Curtiss, L. A.; Raghavachari, K.; Redfern, P. C.; Rassolov, V.; Pople, J. A. *J. Chem. Phys.* **1998**, 109, 7764.
- (37) Lee, T. J.; Taylor, P. R. *Int. J. Quantum Chem. Symp.* **1989**, 23, 199.
- (38) Frisch, M. J.; Trucks, G. W.; Schlegel, H. B. et al. *Gaussian 03*; Gaussian, Inc.: Pittsburgh, PA, 2003.
- (39) DALTON, a molecular electronic structure program, written by Helgaker, T.; Jensen, H. J. Aa.; Joergensen, P.; Olsen, J.; Ruud, K.; Aagren, H.; Auer, A. A. et al., Release 1.2, 2001.
- (40) MOLPRO is a package of ab initio programs written by Werner, H.-J.; Knowles, P. J.; Schütz, M.; Lindh, R.; Celani, P.; Korona, T.; Rauhut,

- G.; Manby, F. R.; Amos, R. D.; Bernhardtsson, A.; Berning, A.; Cooper, D. L.; Deegan, M. J. O.; Dobbyn, A. J.; Eckert, F. et al. 2002.
- (41) Robinson, P.; Holbrook, K. *Unimolecular Reactions*; Wiley-Interscience: London, 1972.
- (42) Forst, W. *Theory of Unimolecular Reactions*; Academic Press: New York, 1973.
- (43) Gilbert, R. G.; Smith, C. S. *Theory of Unimolecular and Recombination Reactions*; Blackwell Scientific: Oxford, 1990.
- (44) Holbrook, K.; Pilling, M.; Robertson, S. *Unimolecular Reactions*, 2nd ed.; Wiley: New York, 1996.
- (45) Steinfeld, J. I.; Francisco, J. S.; Hase, W. L. *Chemical Kinetics and Dynamics*; Prentice-Hall: Englewood Cliffs, NJ, 1999.
- (46) Baer, T.; Hase, W. L. *Unimolecular Reaction Dynamics: Theory and Experiment*; Oxford University Press: Oxford, 1996.
- (47) Beyer, T.; Swinehart, D. F. *Comm. Assoc. Comput. Machines* **1973**, 16, 379.
- (48) Stein, S. E.; Rabinovitch, B. S. *J. Chem. Phys.* **1973**, 58, 2438.
- (49) Hippler, H.; Troe, J.; Wendelken, H. J. *J. Chem. Phys.* **1983**, 78, 6709.
- (50) Troe, J. *J. Chem. Phys.* **1977**, 66, 4745.
- (51) Gillespie, D. T. *J. Comput. Phys.* **1976**, 22, 403.
- (52) Gillespie, D. T. *J. Phys. Chem.* **1977**, 81, 2340.
- (53) Gillespie, D. T. *J. Comput. Phys.* **1978**, 28, 395.
- (54) James, F. *Comput. Phys. Commun.* **1994**, 79, 111.
- (55) Luscher, M. *Comput. Phys. Commun.* **1994**, 79, 100.
- (56) Vereecken, L.; Huyberechts, G.; Peeters, J. *J. Chem. Phys.* **1997**, 106, 6564.
- (57) Herron, J. T.; Huie, R. E. *J. Phys. Chem. Ref. Data* **1973**, 2, 467.
- (58) Gershenzon, Y. M.; Moin, F. B.; Yurkevich, Y. P. *Kinet. Catal.* **1975**, 16, 1192.
- (59) Cvetanovic, R. J. *J. Phys. Chem. Ref. Data* **1987**, 16, 261.
- (60) Malick, D. K.; Petersson, G. A.; Montgomery, J. A., Jr. *J. Chem. Phys.* **1998**, 108, 5704.
- (61) O'Gara, J. E.; Dailey, W. P. *J. Am. Chem. Soc.* **1994**, 116, 12016.
- (62) Tyerman, W. J. R. *Trans. Faraday Soc.* **1969**, 65, 163.
- (63) Hsu, D. S. Y.; Lin, M. C. *Chem. Phys.* **1977**, 21, 235.
- (64) Dunn, K. M.; Morokuma, K. *J. Chem. Phys.* **1995**, 102, 4904.
- (65) Klein, S.; Bearpark, M. J.; Smith, B. R.; M.; Robb, M. A.; Olivucci, M.; Bernardi, F. *Chem. Phys. Lett.* **1998**, 292, 259.
- (66) <http://physics.nist.gov/PhysRefData/Handbook/periodictable.htm>.
- (67) Lee, S. Y.; Yoo, H. S.; Kang, W. K.; Jung, K. H. *Chem. Phys. Lett.* **1996**, 257, 415.
- (68) Yi, H. J.; Jee, Y. J.; Lee, K. W.; Jung, K. H. *Chem. Phys. Lett.* **2000**, 327, 325.
- (69) Kraka, E.; Konkoli, Z.; Cremer, D.; Fowler, J.; Schaefer, H. F. J. *Am. Chem. Soc.* **1996**, 118, 10595.
- (70) Buckley, T. J.; Johnson, R. D.; Huie, R. E.; Zhang, Z.; Kuo, S. C.; Klemm, R. B. *J. Phys. Chem.* **1995**, 99, 4879.